ISSN 2359-6562 (ONLINE) 2359-6562 (CD-ROM)

SENSORIAMENTO REMOTO E SIMULAÇÃO ESTOCÁSTICA NA OBTENÇÃO DE DIFERENTES CENÁRIOS DE EVAPOTRANSPIRAÇÃO

ANDRÉ LUIZ VIANNA DE PAULA[1], DIEGO AUGUSTO DE CAMPOS MORAES[2] E ALEXANDRE DAL PAI[3]

[1] Departamento de Engenharia Rural e Socioeconomia, Universidade Estadual Paulista (UNESP), Faculdade de Ciências Agronômicas, Av. Universitária, 3780, Altos do Paraíso, CEP 18610-034, Botucatu, São Paulo, Brasil, https://orcid.org/0000-0002-4327-3098, alv.paula@unesp.br.
[2] Departamento de Engenharia Rural e Socioeconomia, Universidade Estadual Paulista (UNESP), Faculdade de Ciências Agronômicas, Av. Universitária, 3780, Altos do Paraíso, CEP 18610-034, Botucatu, São Paulo, Brasil, https://orcid.org/0000-0002-1283-901X, diego.c.moraes@unesp.br.
[3] Departamento de Bioprocessos e Biotecnologia, Universidade Estadual Paulista (UNESP), Faculdade de Ciências Agronômicas, Av. Universitária, 3780, Altos do Paraíso, CEP 18610-034, Botucatu, São Paulo, Brasil, https://orcid.org/0000-0002-9194-6875, dal.pai@unesp.br.

RESUMO: Para implementar efetivamente medidas de gestão de recursos hídricos, é fundamental monitorar a evapotranspiração. Consultores da FAO, concluíram que a fórmula de Penman-Monteith foi o método ideal e padrão para a estimativa da ET_o. Um dos métodos indiretos de estimativa da evapotranspiração com sensoriamento remoto é o algoritmo Safer. O objetivo desse trabalho foi a obtenção de diferentes cenários de evapotranspiração na sub-Bacia do alto Rio Pardo-SP utilizando técnicas de sensoriamento remoto e geoestatística. Foram obtidos cenários mínimos, médios e máximos de evapotranspiração para os períodos de 2019, 2020 e 2021. Os maiores valores de evapotranspiração estiveram presentes nas estações da primavera e verão. Porém, no inverno de 2021, houve divergência dos valores comuns. Pesquisas com outros algoritmos como Sebal e Metric podem ser feitas para avaliar a correlação dos dados entre métodos como também a análise dos níveis de precipitação pode corroborar com os valores de evapotranspiração.

Palavras-chaves: evapotranspiração, Safer, geoestatística.

REMOTE SENSING AND STOCHASTIC SIMULATION IN OBTAINING DIFFERENT EVAPOTRANSPIRATION SCENARIOS

ABSTRACT: To effectively implement water resource management measures, monitoring evapotranspiration is essential. FAO consultants concluded that the Penman–Monteith formula was the ideal and standard method for estimating ET_o. One of the indirect methods for estimating evapotranspiration with remote sensing is the Safer algorithm. The objective of this work was to obtain different evapotranspiration scenarios in the upper Rio Pardo-SP subbasin via remote sensing and geostatistical techniques. Minimum, average and maximum evapotranspiration scenarios were obtained for the periods of 2019, 2020 and 2021. The highest evapotranspiration values were present in the spring and summer. However, in the winter of 2021, there was a divergence of common values. Research with other algorithms, such as Sebal and Metric, can be carried out to evaluate the correlation of data between methods, and the analysis of precipitation levels can corroborate the evapotranspiration values.

Keywords: evapotranspiration, Safer, geostatistics.

Recebido em 03/12/2024 e aprovado para publicação em 12/12/2024
DOI: http://dx.doi.org/10.17224/EnergAgric.2024v39p167-176

1 INTRODUCTION

Effective water resource management is highly important from both social and environmental perspectives. Failure to pay attention to this management can compromise the sustainability of natural resource use in a river basin. This is exemplified by the Pardo River Basin in São Paulo, which plays a key role in supplying water to the municipalities of Pardinho and Botucatu. Responsible management of river basins, especially through forest restoration actions, has been recognized as a highly effective and economically viable strategy for conserving water resources. In fact, to effectively implement water resource management measures, monitoring the main elements of the hydrological cycle, with an emphasis on evapotranspiration, which is considered a critical indicator of water loss from the Earth's surface through interactions among soil, vegetation and the atmosphere, is essential.

To estimate the evapotranspiration of agricultural and forestry crops, the best concept is ET_Csince it is necessary to calculate the (Kc)specific crop coefficient for each crop, which is the relationship between ET_o and ET_C. ET_o represents the evapotranspiration rate of a reference surface that does not suffer from water scarcity. This reference surface is modeled from a hypothetical grass crop with specific characteristics. ET_C represents the water loss in healthy, well-nourished crops that are grown in large fields under ideal soil moisture levels and achieve maximum production within certain climatic conditions. Kc evaluated the effects of crop transpiration and soil evaporation on a single coefficient. The main methods for calculating ET_o are Thornthwaite, Camargo, Hargreaves-Samani, Priestley-Taylor and Penman–Monteith. However, after analysis, consultants from the FAO (Food and Agriculture Organization of the United Nations) (Allen *et al*., 1998) concluded that the Penman–Monteith formula was the ideal and standard method for estimating evapotranspiration ET_obecause it is based on physical processes and incorporates physiological and aerodynamic parameters. The Penman–Monteith equation provided an acceptable daily estimate of evapotranspiration for the locations analyzed, even though it presented high values at two points compared with direct methods, such as lysimeters, which are applied to calibrate indirect methods (Allen, 1986). However, direct methods do not meet the demand required for large areas. Thus, the combination of indirect methods such as Penman–Monteith and remote sensing is used to calculate evapotranspiration to expand the scope. Therefore, algorithms have been developed to enable the application of meteorological and orbital data in conjunction to estimate evapotranspiration.

Another essential area of study is geostatistics, which focuses on considering the distances between samples as an essential factor for interpreting observed variations. Therefore, the technique also aims to estimate values in locations where there was no data collection. To assist in the interpretation of data from the execution of algorithms, stochastic simulation, a geostatistical method, is highly beneficial and provides a basis for estimating evapotranspiration scenarios. Therefore, the objective of this work was to obtain different evapotranspiration scenarios in the upper Rio Pardo subbasin (SP) via remote sensing and geostatistical techniques.

2 MATERIALS AND METHODS

The study was carried out in the upper Rio Pardo-SP subbasin (Figure 1), which comprises 5,301 hectares. The area is characterized by the planting of agricultural crops such as corn, soybeans, cassava and forest species, with other agricultural crops on a smaller scale in smaller areas.

Figure 1. Study area

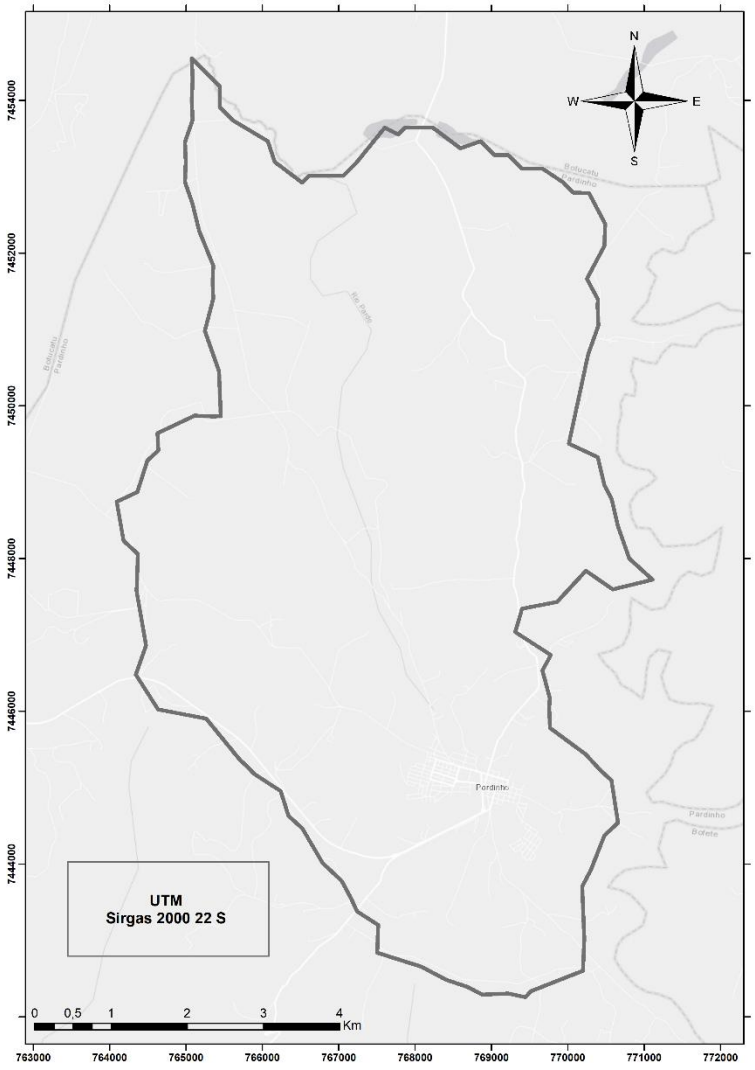

Source: Paula (2023)

The region's climate is mesothermal, with a dry season in winter and classified as Cwa, according to the Köppen classification, with annual median temperatures of approximately 20 °C and precipitation between 1,100 and 1,700 mm per year (Carvalho; Jim, 1983).

The area is composed of soils of the following types: Dystrophic Red Latosol, Dystroferric Red Latosol, Dystrophic Red–Yellow Argisol, Neosol Dystrophic Litholic and Dystrophic Gleysol (Zimback, 1997; Grossi, 2003; Embrapa, 2018). The images used for the study were obtained by the MSI sensor coupled to the Sentinel-2A satellite, which is available at the USGS (2022). Thus, images were collected from the autumn, winter, spring and summer climatic seasons for the periods of 2019, 2020 and 2021, with one image for each season. The images presented a spatial resolution of 10 m, a temporal resolution of 5 days and a radiometric resolution of 12 bits.

The images were selected so that they did not present cloud interference for better quality study of the surface. Therefore, in this study, the cloud-free images for the summer season were all from the year following the one analyzed.

With the images downloaded, the atmospheric correction process began using the dark object subtraction method. Object subtraction (DOS), detailed by Congedo (2018), is the developer of the semiautomatic classification plugin (SCP), which is available in the QGIS software. The next step consisted of starting to apply the equations via the raster

calculator of the same software mentioned above. Safer is a simplified algorithm with good results in the Brazilian territory. It was developed and validated with data from four field experiments of both irrigated crops and natural vegetation (Teixeira *et al.,* 2013a) under semiarid Brazilian conditions, empirically calibrated for the northwestern state of São Paulo and adapted for other regions. This algorithm requires biophysical parameters acquired via remote sensing combined with meteorological data and is applicable to different ecosystems (Teixeira *et al*., 2013b; Franco *et al*., 2022), as is done in Sebal. Safer allows the estimation of ET_C with sensors that do not have a thermal band, requiring the use of the residual method (Teixeira *et al*., 2016). This method uses orbital data together with weather station data (Teixeira, 2010) without the need to choose cold and hot pixels (Teixeira *et al*., 2009). One of the sensors that uses this method is the MSI present in the Sentinel-2A and 2B satellites.

The sequence of equations below was step-by-step for the application of Safer. Initially, the planetary albedo and surface albedo are estimated via Equations 1 and 2, respectively, as proposed by (Teixeira, 2010; Teixeira *et al.,* 2013b; Teixeira *et al.,* 2014).

$$\alpha_p = \sum \omega band . rband \quad (1)$$

where α_p represents the planetary albedo; $\omega band$ represents the weight of each band; and $rband$ represents the narrowband reflectance.

$$\alpha_0 = a . \alpha_p + b \quad (2)$$

where α_0 is the surface albedo and where a and b are regression coefficients for 24-hour periods of 1.70 and 0.13, respectively.

$$NDVI = \frac{(NIR-RED)}{(NIR+RED)} \quad (3)$$

where $NDVI$ is the normalized difference vegetation index and where NIR and RED represent the reflectances in the range of wavelengths in the near-infrared and red regions of the solar spectrum, respectively.

The NDVI index present in the Safer algorithm is highly important for estimating soil moisture and the presence of vegetation since water absorbs all shortwave infrared radiation, and this index is linked to surface moisture. Chlorophyll captures red radiation visible to remote sensors, whereas the spongy mesophyll reflects near-infrared radiation. Therefore, areas with greater photosynthetic activity manifested in satellite images with low reflection at red wavelengths and high reflection at infrared wavelengths (Teramoto *et al*., 2018).

where $Ts\omega$ is the atmospheric shortwave transmissivity, Equation (4). It is defined as the fraction of the solar radiation incident on the top of the atmosphere that reaches the Earth's surface on clear days, that is, without cloud cover. In some studies, it is defined as 44% of the incident radiation on the top of the atmosphere.

$$Ts\omega = \frac{R_{so}}{R_a} \quad (4)$$

where R_{so} represents the solar radiation measured at the Earth's surface on clear days and where R_a represents the incident solar radiation at the top of the atmosphere.

$$\varepsilon_a = aA . (-ln . Ts\omega)^{bA} \quad (5)$$

$$\varepsilon_s = aS . (lnNDVI) + b_s \quad (6)$$

where ε_a and ε_s are the atmospheric and surface emissivities, respectively. The values aA, ^{bA}, aS and b_s are coefficients that, according to Teixeira (2010), are 0.94, 0.10, 0.06 and 1.00, respectively.

The meteorological data were obtained through the automatic meteorological station (EMA) of the Department of Rural Engineering and Socioeconomics of the Faculty of Agronomic Sciences (UNESP) of Botucatu, São Paulo, Brazil, which is located at the coordinates 22 ° 54 'S, 48 ° 27 'W and 786 m. The sensor used to obtain $Tmax$ and $Tmin$ was

a thermistor from the manufacturer Campbell Scientific, which has a sensitivity of 0.1 °C.

$$T_A = \frac{Tmax+Tmin}{2} \quad (7)$$

where T_A is the average air temperature and where $Tmax$ and $Tmin$ (°C) are the maximum and minimum temperatures, respectively.

Equation 8 refers to the longwave radiation balance regression coefficient (Silva; Teixeira; Manzione, 2019; Teixeira *et al*., 2019).

$$aL = c.T_A - d \quad (8)$$

where c and d are regression coefficients equal to 6.99 and 39.93, respectively.

Bastiaanssen *et al*. (1998) used a standard value of aL= 110 without considering local thermal conditions. However, this standard was not used in this study. Therefore, to calculate aL, the value of T_A needs to be converted to °C. To estimate the surface temperature (Ts), the residual method was used (Teixeira *et al*., 2015) since the MSI sensor (Sentinel-2A) does not have a thermal band.

$$Ts = \sqrt[4]{\frac{\varepsilon_a.\sigma.TA^4+aL.Ts\omega}{\varepsilon_s.\sigma}} \quad (9)$$

where Ts is the surface temperature and where σ is the Stefan–Boltzmann constant ($5.67x10^{-8}$ W/m2 K4).

$$Kc = exp\left[e + f\left(\frac{Ts}{\alpha_0 * NDVI}\right)\right] \quad (10)$$

where Kc is the culture coefficient and where e and f are regression coefficients of 1.8 and −0.008, respectively.

The value of Ts was also applied at °C in this case. Equations 11 and 12 display the reference crop evapotranspiration (ET_o) and the crop evapotranspiration under standard conditions (ET_C), respectively. These equations are in the daily partition (mm.day $^{-1}$) (Allen *et al*., 1998).

$$ET_o = \frac{0.408.\Delta.(Rn-G)+\left[y\frac{900}{T+273}.u_2.(e_s-e_a)\right]}{\Delta+y.(1+0.34.u_2)} \quad (11)$$

where Rn represents the net radiation (MJ.m $^{-2}$.day); G represents the sensible heat flux conducted to the ground (MJ.m $^{-2}$.day); T represents the average daily air temperature (°C); u_2 represents the wind speed at 2 m (ms $^{-1}$); e_s represents the vapor pressure of saturated air (kPa); e_a represents the real vapor pressure of the air (kPa); Δ represents the gradient of the vapor pressure curve of the air in the atmosphere (kPa °C $^{-1}$); and y represents the psychometric constant (kPa.°C $^{-1}$).

u_2The same station was used, and the element/sensor was a set of 3 mugs (Campbell Scientific) with a sensitivity of 0.12 ms $^{-1}$.

$$ET_C = \text{Kc}.ET_o \quad (12)$$

where ET_C represents crop evapotranspiration under standard conditions and where ET_o represents reference crop evapotranspiration (mm.day-¹).

With the values ET_Cobtained throughout the basin for all seasons, it was possible to apply geostatistical techniques to obtain different evapotranspiration scenarios (minimum, average and maximum) according to the objective of the study. To estimate spatial dependence, the steps applied must be variogram, cross-validation, kriging and stochastic simulation, in that order. The steps were applied through the *geostatistical tool Analyst* available in ArcGIS 10.3 software. First, descriptive statistics were performed to obtain the minimum, mean, maximum, standard deviation and asymmetry of the values. Soon after, with the same software, the geostatistical wizard was used to apply kriging. Simple kriging was used to meet the requirement for executing the Gaussian sequential simulation, which uses data with a normal distribution as input data. To correct the smoothing of the data resulting from the kriging process, the SSG stochastic simulation was subsequently applied. Therefore, the

exponential variogram and the cross-validation necessary for its validation were applied. The parameters observed in the cross-validation were the Pearson correlation coefficient (r) and EM (Mukaka, 2012; Cochran, 1977). In this way, the values of the nugget effect, plateau, reach and GDE were obtained with greater precision. The sequential Gaussian simulation was applied by estimating 100 realizations within each pixel of the images obtained through the MSI sensor coupled to the Sentinel-2A satellite to obtain the ranges of minimum, maximum and average evapotranspiration values for the upper Rio Pardo subbasin-SP.

3 RESULTS AND DISCUSSION

For descriptive statistics, the highest evapotranspiration values for the years 2019, 2020 and 2021 were found in the spring season, with values of 17.09 (Table 6), 15.88 (Table 7) and 14.92 (Table 8) (mm.day-[1]), respectively.

Table 6. Descriptive statistics 2019

Seasons of the year	Min. Etc/mm.day^{-1}	Average Etc/mm.day^{-1}	Max. Etc/mm.day^{-1}	Pad Dev .	Asymmetry
Fall	0	5.10	9.97	2.19	-0.80
Winter	0	4.43	9.30	2.33	-0.25
Spring	0	4.67	17.09	4.18	0.40
Summer	0	7.71	15.88	3.95	-0.60

Min: Minimum; Max: Maximum; Std. Dev: Standard deviation.
Source: Paula (2023)

Table 7. Descriptive statistics 2020

Seasons of the year	Min. Etc/mm.day^{-1}	Average Etc/mm.day^{-1}	Max. Etc/mm.day^{-1}	Pad Dev .	Asymmetry
Fall	0	5.67	10,11	2.39	-0.70
Winter	0	4.12	8.41	1.92	-0.33
Spring	0	6.01	18.93	5.16	0.42
Summer	0	9.11	13.99	3.04	-1.26

Min: Minimum; Max: Maximum; Std. Dev: Standard deviation.
Source: Paula (2023)

Table 8. Descriptive statistics 2021

Seasons of the year	Min. Etc/mm.day^{-1}	Average Etc/mm.day^{-1}	Max. Etc/mm.day^{-1}	Pad Dev .	Asymmetry
Fall	0	6.48	12.82	3.15	-0.59
Winter	0	5.31	14.66	3.41	0.29
Spring	0	4.22	14.92	3.95	0.43
Summer	0	6.45	11.71	2.92	-0.66

Min: Minimum; Max: Maximum; Std. Dev: Standard deviation.
Source: Paula (2023)

The variogram analysis, the seasons and periods with the lowest nugget effect and consequently the lowest and best GDE were summer 2019 (nugget effect of 0.06 and GDE of 0.07), spring 2020 (nugget effect of 0.06 and GDE of 0.06) and summer 2021 (nugget effect of 0.01 and GDE of 0.01). Finally, the variograms in the studied periods presented moderate to strong spatial dependence. The summer 2021 period presented lower nugget effect values, characterizing the most pronounced spatial dependence among the

samples. The nugget effect is derived from the small-scale variability not obtained or caused by measurement failures or, in other words, a positive value that presents the lack of continuity of the semivariogram at distances shorter than the smallest distance reported in the samples.

With respect to cross-validation, the Pearson correlation method was applied due to the normal distribution of the variables studied, with 1/3 of the actual sample being validated. The correlation method is a way of estimating a possible association between a pair of variables. This is a statistical methodology that can alternate between -1 (absolute negative), 0 (no correlation), and 1 (absolute positive correlation). If the results are positive numbers, the variables are considered directly proportional (one increases the other as well). However, if the results are negative, the variables will have inversely proportional characteristics (one increases and the other decreases). In this study, values close to 1 for cross-validation were observed in all periods. The lowest value occurred in the fall of 2020 (0.96), and the highest value occurred in the summer of 2021 (0.99). The EM presented minimum values between -0.07 and -0.03 in the fall and winter seasons of 2020, in that order. Negative EM values indicate overestimation of the results, and positive values indicate underestimation. This study revealed overestimation of the results, but to a slight degree. Both EM and Pearson's correlation methods are methodologies responsible for validating the results and determining whether there was a good adjustment of the variogram, which is a baseline condition for the quality of the data collected. However, in this study, both criteria were offered.

Finally, for the 100 SSG achievements, the highest evapotranspiration rates occurred in the seasons with the highest incidence rates of radiation (spring and summer) in the three years of study. However, in the winter of 2021, as shown in Figure 2, this metric diverged, presenting values higher than usual for the season; one of the possible causes is the presence of exposed soil and high precipitation, since the latter considerably increases the evapotranspiration rate because it is intrinsically linked to the availability of water in the soil. The maximum evapotranspiration values for the winter season in the periods of 2019 and 2020 were 11.69 mm.day-^{1} and 11.02 mm.day-^{1}, respectively. However, the values presented in the SSG were an estimate of the evapotranspiration values pixel by pixel, where they also evaluated points where there was no crop, such as paved urban areas, because the shape of the image covers the basin area homogeneously. Thus, high evapotranspiration values could also be explained by the presence of urban areas in the image studied, which were classified only as evaporation.

Figure 2. Evapotranspiration map for winter 2021 (ET_C)

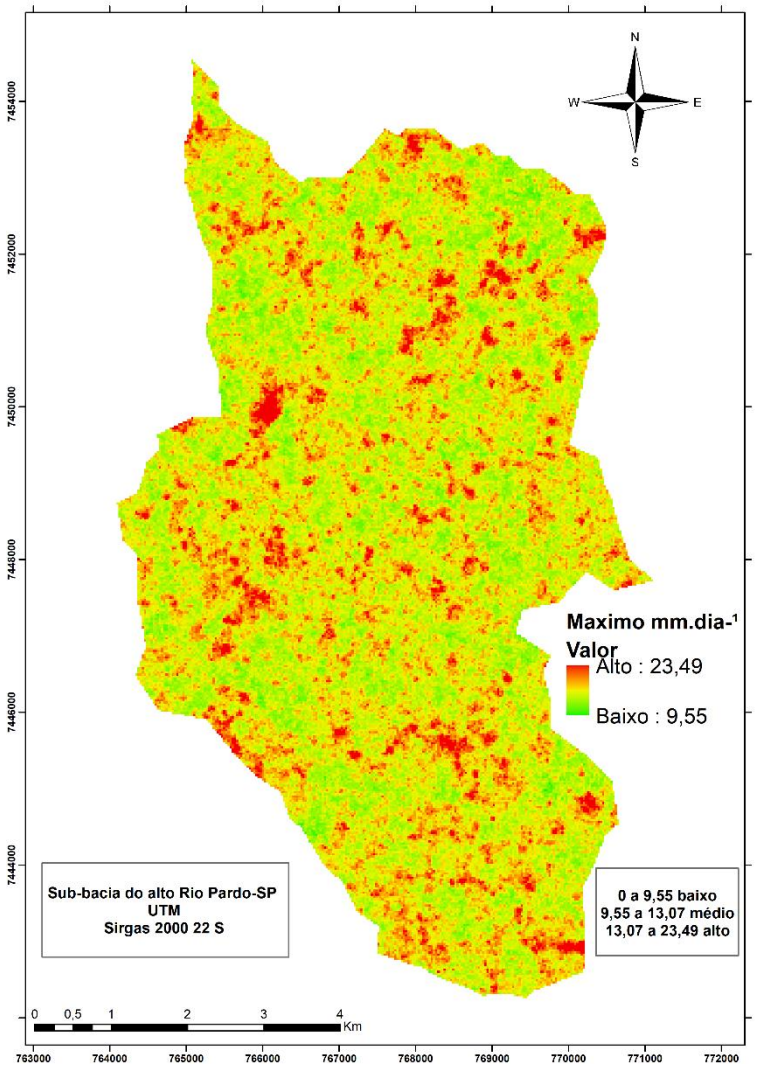

Source: Paula (2023)

4 CONCLUSIONS

The Safer algorithm together with geostatistical techniques provides satisfactory evapotranspiration results.

It was possible to estimate the evapotranspiration of the upper Rio Pardo subbasin in São Paulo and consequently contribute to local agriculture and preservation of natural resources. Future studies may estimate the irrigation depth for agricultural crops in the area on the basis of the data obtained.

Since remote sensing is an analysis technique without physical contact with an object, to accurately assess the causes of evapotranspiration values, *onsite analysis is necessary*. In addition, to ensure the accuracy of the method used, research with other algorithms, such as Sebal and Metric, can be carried out to assess the correlation of data between methods, and the analysis of precipitation levels in the periods studied can corroborate the evapotranspiration values obtained.

5 REFERENCES

ALLEN, RG A Penman for all seasons. **Journal of Irrigation and Drainage Engineering** , Reston, vol. 112 , no. 4, p. 348-368, 1986.

ALLEN, RG; PEREIRA, LS; RAES, D.; SMITH, M. **Crop evapotranspiration** : guidelines for computing crop requirements. Rome: FAO, 1998. (Irrigation and Drainage Paper, n. 56).

BASTIAANSSEN, WGM; MENENTI, M.; FEDDES, RA; HOLTSLAG, AAM A remote sensing surface energy balance algorithm for land (SEBAL) - 1. Formulation . **Journal of Hydrology ,** Glendale, vol. 212/213, p. 198-212, 1998.

CARVALHO, WA; JIM, J. **Environmental protection areas** : "Serra de Botucatu" Region and "Serra de Fartura" Region. Botucatu: Basic Institute of Biology , 1983.

COCHRAN, W. G. **Sampling Techniques** . 3rd ed. New York: John Wiley & Sons, 1977.

CONGEDO, L. **Semiautomatic classification plugin documentation.** Release 5.3.6.1. Luca Congedo , 2018. Available at: https://readthedocs.org/projects/semiautomaticclassificationmanual-v5/downloads/pdf/latest/. Accessed on: July 14, 2022.

FRANCO, JR; RANIEIRO, MR; CALÇA, MVC; RODRIGUES, SA; DAL PAI, A.; DAL PAI, E. Comparative Analysis Between Meteorological Measurements of the Conventional and Automatic Station of the Lageado Farm in the Municipality of Botucatu, São Paulo, Brazil. **Brazilian Journal of Meteorology** , Rio de Janeiro, v. 37, n. 2, p. 223-232, 2022.

GROSSI, CH **Geographic information system - Basins 3.0 in the hydrological modeling of the experimental basin of Rio Pardo, SP** . 2003. Dissertation (Master in Agronomy/Energy in Agriculture) – Faculty of Agronomic Sciences, São Paulo State University, Botucatu, 2003.

MUKAKA, MM Statistics Corner: A guide to appropriate use of Correlation coefficient in medical research. **Malawi Medical Journal**, Blantyre, vol. 24, no. 3, p. 69-71, 2012.

PAULA, ALV **Remote sensing and stochastic simulation to obtain different evapotranspiration scenarios** . 2023. Dissertation. (Master in Agricultural Engineering) – Faculty of Agricultural Sciences, São Paulo State University, Botucatu, 2023.

EMBRAPA. **Brazilian soil classification system** . 5th ed. rev. and ampl . Brasília, DF: Embrapa, 2018.

SILVA, COF; TEIXEIRA, AHC; MANZIONE, RL Agriwater: An R package for spatial modeling of energy balance and current evapotranspiration using satellite images and agrometeorological data. **Environmental Modeling and Software** , v. 120, p. 1-19, 2019.

TERAMOTO, EH; BENJUMEA, MT; GONÇALVES, RD; KIANG, CH **Brazilian Cartography Magazine** , City, v. 70, n. 3, p. 1135-1157, 2018.

TEIXEIRA, AHC; MIRANDA, FR; LEIVAS. JF; PACHECO, EP; GARÇON, EAM Water productivity assessments for dwarfs coconut by using Landsat 8 images and agrometeorological data. **ISPRS Journal of Photogrammetry and Remote Sensing** , Waltham , v. 155, p. 150-158, 2019.

TEIXEIRA, AHC Determining regional current evapotranspiration of irrigated crops and natural vegetation in the São Francisco river basin (Brazil) using remote sensing and Penman–Monteith equation. **Remote Sensing** , Basel, v. 2, no. 5, p. 1287-1319, 2010.

TEIXEIRA, AHC; BASTIAANSSEN, WGM; AHMAD, MD; BOS, MG Reviewing SEBAL input parameters for assessing evapotranspiration and water productivity for the Low -Middle São Francisco River basin , Brazil Part B: Application to the regional scale . **Agricultural and Forest Meteorology**, v. 149, n. 3/4, p. 477-490, 2009.

TEIXEIRA, AHC; LEIVAS, JF; RONQUIM, CC; VICTORIA, DC Sugarcane Water Productivity Assessments in the São Paulo state , Brazil . **International Journal of Remote Sensing Applications** , Philadelphia, vol. 6, p. 84-95, 2016.

TEIXEIRA, AHC; HERNANDEZ, FBT; ANDRADE, RG; LEIVAS, JF; BOLFE, EL Energy balance with Landsat images in irrigated central pivots with corn crop in the São Paulo State, Brazil. **Proceedings of SPIE**, Bellingham, vol. 9239, p. 92390O-1-92390O-10, 2014.

TEIXEIRA, AHC; HERNANDEZ, FBT; LOPES, HL; SCHERER-WARREN, MS; BASSOI, LH Spatiotemporal modeling of energy and water balance components in the Brazilian semiarid region. **Embrapa Satellite Monitoring**, Campinas, Documents 99, p. 1-32, 2013a.

TEIXEIRA, AHC; PADOVANI, CR; ANDRADE, RG; LEIVAS, JF; VICTORIA, DC; GALDINO, S. Use of MODIS images to quantify the radiation and energy balances in the Brazilian pantanal . **Remote Sensing**, Basel, v. 7, no. 11, p. 14597-14619, 2015.

TEIXEIRA, A.H.C.; SCHERER-WARREN, M.; HERNANDEZ, FBT; ANDRADE, R. G .; LEIVAS, J.F. Large- Scale Water Productivity Assessments with MODIS Images in a Changing Semi-Arid Environment : A Brazilian Case Study . **Remote Sensing,** Basel, vol. 5, no. 11, p. 5783-5804, 2013b.

USGS. **EarthExplorer** . Washington, DC: USGS, 2022. Available at: https://earthexplorer.usgs.gov/ . Accessed: July 8, 2022.

ZIMBACK, CRL **Semidetailed survey of the soils of the Rio Pardo basin in the municipalities of Pardinho and Botucatu**. Botucatu: FEPAF, 1997.